Progress In Electromagnetics Research Letters, Vol. 102, 1–8, 2022

Bandpass Frequency Selective Surface with Sharp Sidebands for 5G Electromagnetic Shielding of Fixed Satellite System in C-Band

Min Tang*, Qi-Kun Liu, Dong-Fang Zhou, Chen-Qing Pan, and Zhen-Ning Yao

Abstract—In this letter, a new bandpass frequency selective surface (FSS) with sharp sidebands is proposed to suppress electromagnetic interferences caused by the fifth generation (5G) mobile communication to fixed C-band satellite system. The proposed design is composed of three cascaded layers separated by air space, whose unit cell geometry comprises metal square loops, square slots, and their evolvement. As the overall configuration yields high-order bandpass characteristics with multiple transmission poles and zeros, a flat passband covering 3.7–4.2 GHz is obtained, while the out-of-band shielding effectiveness mostly remains better than 20 dB over frequency lower than 6.5 GHz. Good angular stability and polarization independency are also achieved due to structural symmetry. A prototype was fabricated and measured, whose results agree well with the full-wave simulation.

1. INTRODUCTION

The era of emerging telecommunication technology, referred to as the Fifth Generation of Wireless Networks (5G), has arrived. The Third Generation Partnership Project (3GPP) has allocated two main frequency ranges for spectrum of 5G, including frequency range 1 (FR1) from 0.45 GHz to 6.0 GHz and frequency range 2 (FR2) from 24.25 GHz to 52.6 GHz [1]. However, currently the standard C-band (3.7–4.2 GHz) is utilized for downlink frequency of fixed satellite services (FS) [2, 3]. Low frequency-band 5G signals received by the fixed satellite receiving station cause excessive input power, leading to saturation jamming or barrage jamming, which may even damage the FS devices [4].

To suppress interferences to FS caused by 5G, several measures can be taken. The first is to make use of antenna directivity by changing the construction location of 5G base stations to evade the main lobe of FS. The second is to lower the transmit power of 5G base stations by installing metal shielding net and adjusting their maximum radiation direction as well as inclination angle. The third is to retrofit frequency filters with high isolation into the FS receiving stations, which is a more adaptable and effective approach than the former two [5, 6]. Considering that the frequency selective surface (FSS) exhibits filtering characteristics to spatial incident electromagnetic waves (EMW), it can be applied in spatial signal preprocessing for C-band FS to attenuate interferences. In order to reject the out-of-band interference and ensure that the in-band signals transmit with low loss simultaneously, bandpass FSS with flat passband, sharp sideband,s and wide out-of-band rejection is generally best suited.

In the interests of high selectivity, [7] and [8] took advantage of coupling between the slot resonance and the fundamental or high-order resonate modes in substrate integrated waveguide (SIW) cavities, presenting steep roll-off at one side of passband. On this basis, [9] obtained two sharp sidebands to the co-polarized incident EMW by increasing the number of slot resonances, which minimized the unit dimension with application of half resonate mode. Recently, three dimensional FSS has also been investigated to realize quasi-elliptic filtering performance with fast roll-off [10, 12]. Despite the

Received 20 October 2021, Accepted 16 December 2021, Scheduled 25 December 2021

* Corresponding author: Min Tang (tangminmvp@126.com).

The authors are with the National Digital Switching System Engineering and Technological Research Center, Zhengzhou 450001, China.

compact unit cell, difficulties in fabrication and implementation deteriorate its feasibility and flexibility [13]. Antenna-filter-antenna FSS has also been investigated by some researchers [14, 15]. Although electromagnetic coupling through aperture enables the configurations to present flat passband or steep sidebands, the studies were limited to high frequency performance till now. In addition, [16] and [11] cascaded several single-layer FSSs and separated them with air space, which achieved high-order filter characteristics with concise principle.

To obtain low loss to the fixed satellite in C-band and provide electromagnetic shielding for 5G in FR1, this paper presents a new bandpass FSS by cascading three single layers, which are separated by air space. The unit cell geometry is composed of gridded square loops, square slots, and their evolvement, presenting high-order bandpass characteristics with multiple transmission poles and zeros to improve the selectivity. As a result, a flat passband covering C-band with steep roll-off is obtained, while angular stability and polarization independence are also achieved due to symmetric configuration. Equivalent circuit model is established to analyze the working principle. Eventually, performance of the proposed design is verified by both simulation and experimental measurements.

2. DESIGN AND ANALYSIS

2.1. Unit Geometry Design

To obtain high-order characteristics that are easy for FSS configuration to realize, an equivalent circuit model (ECM) is established in Fig. 1 at first. In the ECM, the parallel LC resonators are formed by cascaded multilayer FSS, while the transmission lines are equivalent to air space.

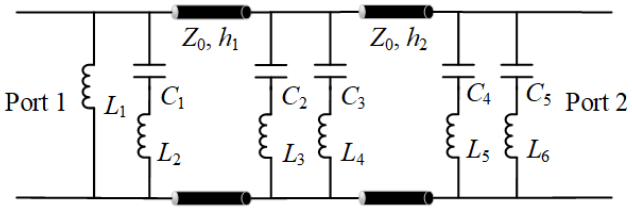

Figure 1. Unit cell geometry of the proposed FSS.

Accordingly, in the top layer, the series resonator L_2C_1 presents one transmission zero (TZ) at f_{z1} while the parallel resonator $L_1L_2C_1$ presents one transmission pole (TP) at f_{01}, which is calculated as follows

$$f_{z1} = \frac{1}{2\pi\sqrt{L_2C_1}} \tag{1}$$

$$f_{01} = \frac{1}{2\pi\sqrt{(L_1+L_2)C_1}} \tag{2}$$

As for the middle layer, two series LC resonators L_3C_2 and L_4C_3 present two TZs at f_{z2} and f_{z3}, respectively. And one TP at f_{02} is yielded by the overall parallel resonator. The resonant frequencies are obtained as

$$f_{z2} = \frac{1}{2\pi\sqrt{L_3C_2}} \tag{3}$$

$$f_{z3} = \frac{1}{2\pi\sqrt{L_4C_3}} \tag{4}$$

$$f_{02} = \frac{1}{2\pi\sqrt{(L_3+L_4)C_2C_3/(C_2+C_3)}} \tag{5}$$

Equally, in the bottom layer, two TZs at f_{z4} and f_{z5}, and one TP at f_{03} are presented, which are

$$f_{z4} = \frac{1}{2\pi\sqrt{L_5C_4}} \tag{6}$$

$$f_{z5} = \frac{1}{2\pi\sqrt{L_6 C_5}} \tag{7}$$

$$f_{03} = \frac{1}{2\pi\sqrt{(L_5 + L_6)C_4 C_5/(C_4 + C_5)}} \tag{8}$$

According to the theory of transmission line model, the air space should act as a quarter-wavelength impedance transformer. In order to obtain a flat passband, f_{01}, f_{02}, and f_{03} should be located in C-band with close but different values. On the other hand, to obtain sharp sidebands, TZs should distribute at both sides near the passband. Considering that the closed-form solution of equivalent circuit parameters cannot be derived from the FSS unit geometry with calculative formulae, quantitative calculation has limited effects. Thus, only qualitative analysis is completed to guide the FSS design here, based on which the corresponding composite unit cell topology is demonstrated in detail in Fig. 2.

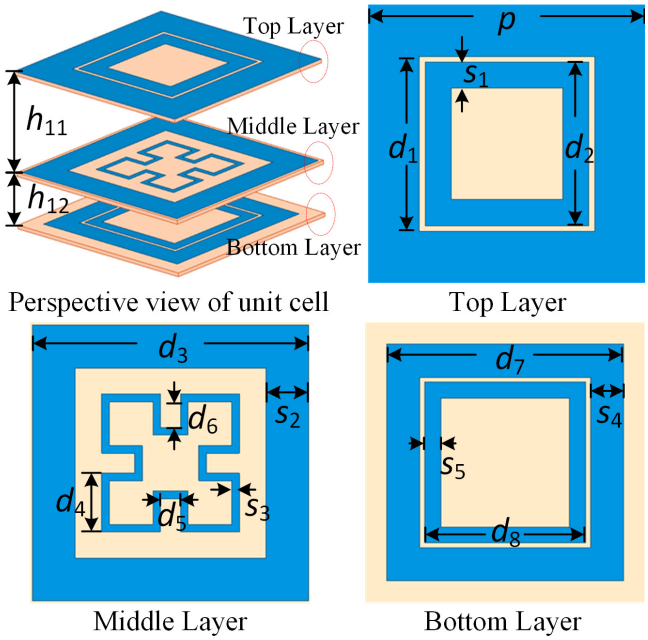

Figure 2. Equivalent circuit model of the proposed FSS.

Specifically, the top layer comprises one gridded square loop, where the external grid and internal loop are equivalent to L_1 and L_2, respectively. The slot between the loops forms gap capacitance C_1 which is in series with L_2. And the series resonator L_2C_1 is in parallel with L_1. The middle layer comprises two coaxial square loops, where the internal one is convoluted so as to increase the equivalent electrical length. Gap between the two adjacent units forms gap capacitance C_2 which is in series with L_3 formed by the external loop. In addition, the slot between two loops forms C_3 which is in series with L_4 formed by the internal loop. The bottom layer also comprises two coaxial square loops. Thus, similarly the external loop forms L_5 in series with gap capacitance C_4, while the internal loop forms L_6 in series with capacitance C_4 formed by the slot.

With the analysis, parameters of the unit cell geometry are deliberately adjusted so that the ECM manages to meet the requirements above, which are listed in Table 1. All the configurations are backed by substrates made of F4BM with the thickness of 0.5 mm ($\varepsilon_r = 2.2$, $\tan\delta = 0.017$). Parameters of the final ECM are calculated and demonstrated in Table 2.

2.2. Simulated Performance and Analysis

The proposed FSS is simulated in CST Microwave Studio with Floquet ports, periodic boundary conditions, and frequency domain solver under different polarizations and oblique incidence from 0.1 GHz

Table 1. Parameters of the proposed FSS.

Parameter	p	d_1	d_2	d_3	d_4	d_5	d_6	d_7
Value (mm)	30	20.6	17.5	29.2	6.2	2	2.7	26.6
Parameter	d_8	s_1	s_2	s_3	s_4	s_5	h_{11}	h_{12}
Value (mm)	17	1.4	3.2	0.8	3	1.7	13	3.5

Table 2. Parameters of the ECM.

Parameter	L_1	L_2	L_3	L_4	L_5	L_6
Value (nH)	4.46	5.89	6.59	8.23	9.26	3.03
Parameter	C_1	C_2	C_3	C_4	C_5	
Value (pF)	0.16	0.85	0.13	0.33	0.22	

to 6.5 GHz.

In Fig. 3, scattering characteristics of the proposed design obtained with electromagnetic simulation in CST and ECM simulation in ADS are contrasted, and the good agreement between them verifies the proposed FSS. Moreover, according to full-wave EM simulation results, the −3 dB passband with insertion loss (IL) less than 3 dB covers 3.71–4.23 GHz with fraction bandwidth of 13.1%, while the −1 dB passband covers 3.79–4.20 GHz. The ratio $\mathrm{BW}_{1\,\mathrm{dB}}/\mathrm{BW}_{3\,\mathrm{dB}} = 0.79$ indicates that the proposed FSS presents a flat passband. The transition band is defined as a frequency range where the transmission coefficient monotonically changes from −3 dB to −10 dB or conversely. According to the definition, the two transitional bandwidths are 210 MHz and 40 MHz, respectively. Thus, steep roll-off at both sides of passband is observed. In addition, the stopband whose rejection characteristic is more than 20 dB covers 0.1–0.62 GHz, 1.51–3.22 GHz, and 4.59–6.5 GHz, verifying the existence of wide out-of-band rejection.

Figure 4 demonstrates performance of the proposed FSS for different polarization angles ϕ under normal incidence. As good agreements between different curves are observed, polarization independence of the design is verified.

Figures 5(a) and 5(b) demonstrate performance of the proposed FSS for oblique incidence θ under TE and TM polarizations, respectively. Based on Fig. 5, it is found that performance of the flat passband remains stable for dual-polarization with $\theta < 40°$. In addition, bandwidth of the passband decreases slightly with oblique incident angle for TE-polarized EMW, while it increases slightly with

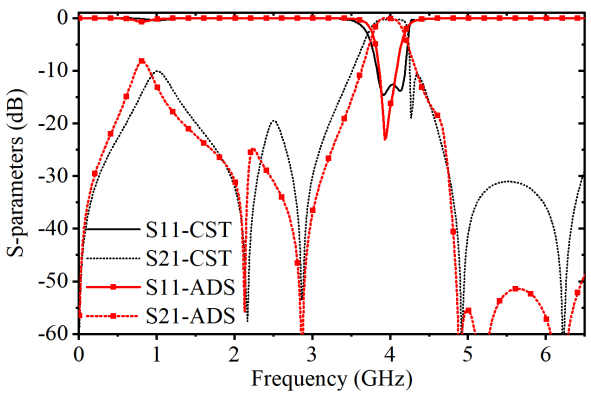

Figure 3. Comparison between simulation results in CST and ADS.

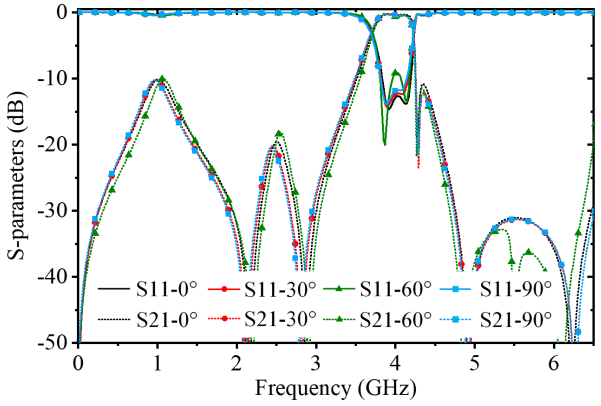

Figure 4. Simulated scattering parameters under different polarizaiton angles.

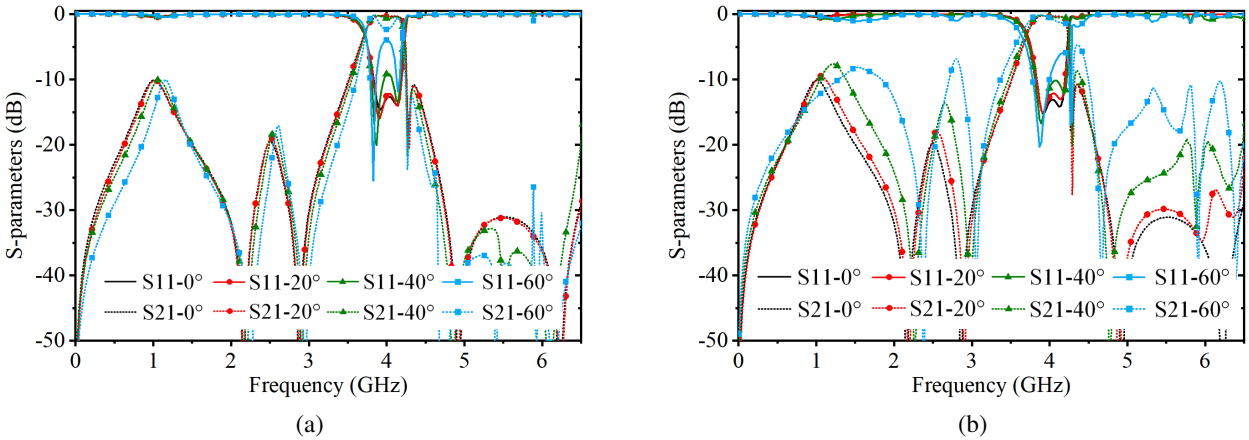

Figure 5. Simulated scattering parameters for oblique incidence under (a) TE polarization and (b) TM polarization.

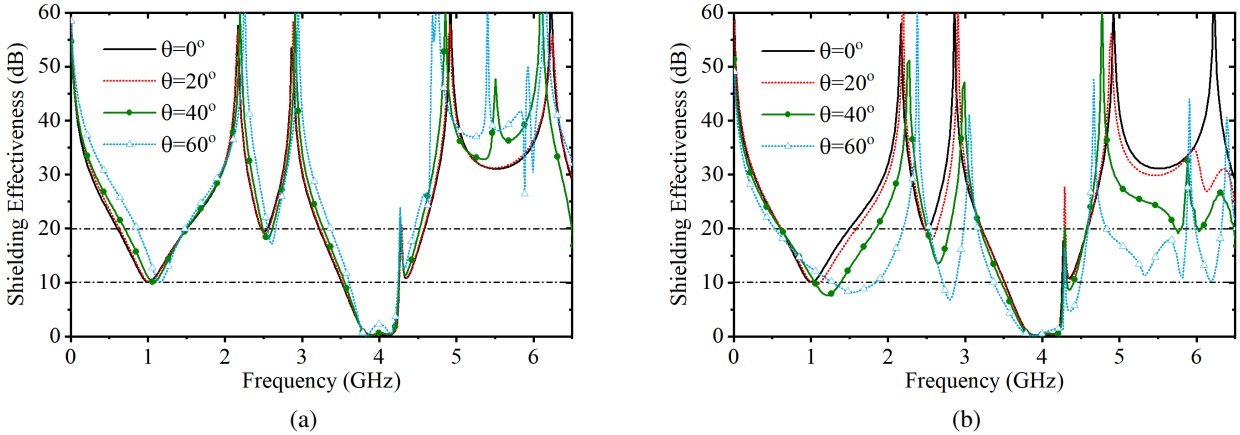

Figure 6. Simulated shielding effectiveness for oblique incidence under (a) TE polarization and (b) TM polarization.

oblique incident angle for TM-polarized EMW.

In Fig. 6, shielding effectiveness (SE) for oblique incidence under dual polarizations is investigated, where SE is defined as

$$\mathrm{SE_{dB}} = -20 \times \log_{10}(\mathrm{S_{transmission}}) \tag{9}$$

According to Fig. 6, SE of the stopbands is mostly better than 20 dB. For TE-polarized EMW, SE performs stably with $\theta < 60°$, while for TM-polarized EMW SE shows stability with $\theta < 40°$.

3. EXPERIMENTAL VERIFICATION AND DISCUSSION

To verify the proposed bandpass FSS, a prototype, which consists of 10×10 unit elements and covers 32 cm $\times$ 32 cm, was fabricated and measured as shown in Fig. 7. Free space measurement was applied in an anechoic chamber constructed by foam absorbers with two pyramid horn antennas as transmitter and receiver. Besides, a vector network analyzer form Aglilent was utilized to measure the performance over 0.5–6.5 GHz.

Figure 8 contrasts the measured and simulated transmission coefficients for normal incidence. According to the experimental results, a -3 dB passband ranging from 3.7 GHz to 4.17 GHz is obtained with relative bandwidth of 11.9%, while two transitional bandwidths are 190 MHz and 90 MHz,

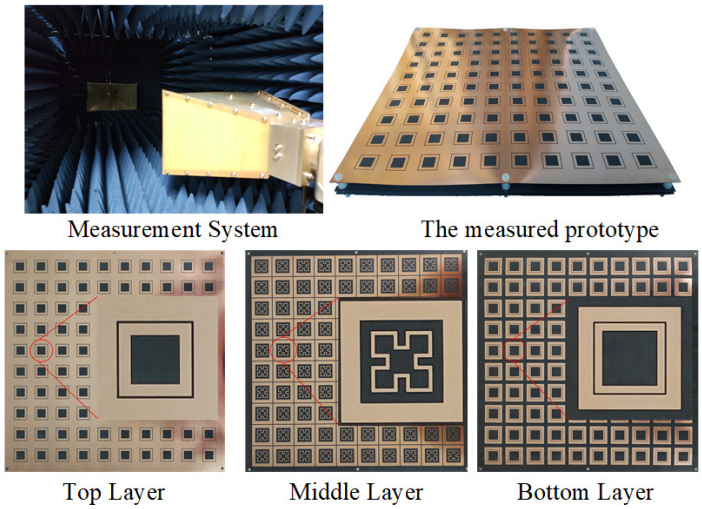

Figure 7. Measurement system and the fabricated prototype.

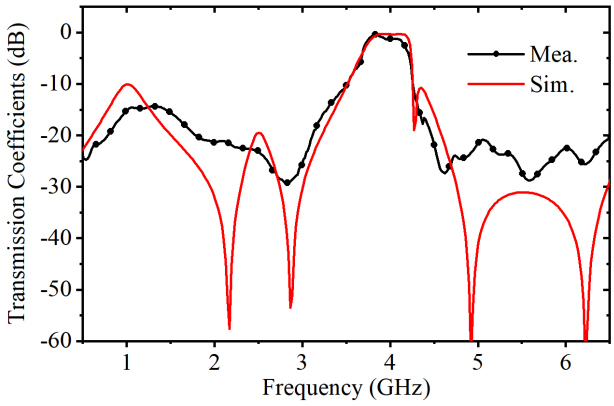

Figure 8. Measured and simulated transmission coefficients for normal incidence.

Table 3. Parameters of the ECM.

Reference	Stopband (GHz)	Passband (GHz)	Polarization	Angular stability
[9]	0.1–4.1 (190%) 4.86–9.8 (67.5%)	4.32–4.84 (11.3%)	Single	45°
[12]	0.1–2.86 (186.5%) 3.42–4.18 (20%)	2.91–3.21 (9.8%)	Dual	40°
[14]	0.1–11.75 (196.6%) Not discussed	12.35–14.78 (17.9%)	Dual	40°
[11]	0.1–4.4 (191%) 5.7–10.2 (56.6%)	4.8–5.4 (11.8%)	Dual	40°
This Work	0.1–3.5 (189%) 4.27–7.1 (49.8%)	3.71–4.23 (13.1%)	Dual	40°

respectively. As for the stopbands whose SE is better than 20 dB, they cover 0.5–0.78 GHz, 1.79–3.1 GHz, and 4.47–6.5 GHz. The good agreement between the measurement and simulation results verifies the flat passband, steep roll-off, and wide out-of-band rejection characteristics of the proposed design. The differences between them may attribute to manufacture tolerance, finite period of FSS, and ohmic loss of the metal sheets.

In Table 3, performances of the proposed FSS and similar reported researches are compared. Despite the increase in thickness, the proposed design achieves highly selectivitive bandpass characteristics in C-band with wide out-of-band rejection.

4. CONCLUSION

Considering interferences of 5G to the C-band fixed satellite receiver, a new bandpass FSS is proposed for electromagnetic shielding. As the cascaded three layers based on fundamental and evolvement of square loops and slots are applied to present high-order filtering characteristics, three close transmission poles in the transmission band improve the passband flatness, while the two transmission zeros near the passband achieve two sharp sidebands. Moreover, multiple transmission zeros in the stopbands yield wide out-of-band rejection, whose shielding effectiveness is better than 20 dB mostly. Angular stability and polarization independence are also obtained due to structural symmetry. Since the passband covers the standard C-band and the stopband covers the rest of low-frequency range in 5G, the proposed design can be a competitive candidate for antenna radome of the fixed satellite receiver.

ACKNOWLEDGMENT

This work was supported by the National Natural Science Foundation of China under Grant 61871405.

REFERENCES

1. 38104-f00, [Online]. Available: https://www.3gpp.org/ftp/Specs/archive/38series/38.104/.
2. Guidolin, F. and M. Nekovee, "Investigating spectrum sharing between 5G millimeter wave networks and fixed satellite systems," *IEEE Globecom Workshops (GC Wkshps)*, 1–7, 2015.
3. Qu, M., Y. F. Feng, and J. Su, and S. M. A. Shah, "Investigating spectrum sharing between 5G millimeter wave networks and fixed satellite systems," *IEEE Globecom Workshops (GC Wkshps)*, 1–7, 2015.
4. Zhang, J. H., L. P. Yan, R. Gao, C. G. Wang, and X. Zhao, "A novel 3D ultra-wide stopband frequency selective surface for 5G electromagnetic shielding," *2020 International Symposium on Electromagnetic Compatibility — EMC EUROPE*, 1–4, 2020.
5. Yew, C. E., C. Y. Choon, M. Y. Alias, and L. S. Wei, "Fixed satellite service and broadband wireless access interference analysis in the extended C-band," *2011 IFIP Wireless Days (WD)*, 1–3, 2011.
6. Li, D., T. W. Li, R. Hao, H. S. Chen, W. Y. Yin, H. C. Yu, and E. P. Li, "A low-profile broadband bandpass frequency selective surface with two rapid band edges for 5G near-field applications," *IEEE Trans. Electromagnetic Compatibility*, Vol. 59, No. 2, 670–676, 2017.
7. Krushna, K. V. and S. Raghavan, "EM design and analysis of frequency selective surface based on substrate-integrated waveguide technology for airborne radome application," *IEEE Trans. Microw. Theory Techn.*, Vol. 67, No. 5, 1727–1739, 2019.
8. Krushna, K. V. and S. Raghavan, "Design of SIW cavity models to control the bandwidth of frequency selective surface," *IET Microw. Antennas Propag.*, Vol. 13, No. 14, 2515–2524, 2019.
9. Yang, L. L., X. C. Wei, D. Yi, and J. M. Jin, "A bandpass frequency selective surface with a low cross-polarization based on cavities with a hybrid boundary," *IEEE Trans. Antennas Prppag.*, Vol. 65, No. 2, 654–661, 2017.
10. Li, B. and Z. X. Shen, "Three-dimensional bandpass frequency-selective structures with multiple transmission zeros," *IEEE Trans. Antennas Prppag.*, Vol. 61, No. 10, 3578–3589, 2013.

11. Li, B. and Z. X. Shen, "Synthesis of quasi-elliptic bandpass frequency-selective surface using cascaded loop arrays," *IEEE Trans. Antennas Prppag.*, Vol. 61, No. 6, 3053–3059, 2013.
12. Zhu, J. P., W. C. Tang, C. Wang, C. Huang, and Y. R. Shi, "Dual-polarized bandpass frequency-selective surface with quasi-elliptic response based on square coaxial waveguide," *IEEE Trans. Antennas Prppag.*, Vol. 66, No. 3, 1331–1339, 2018.
13. Rashid, A. K., B. Li, and Z. X. Shen, "An overview of three-dimensional frequency-selective structures," *IEEE Antennas Propag. Magazine*, Vol. 56, No. 3, 43–67, 2014.
14. Xie, J. M., B. Li, Y. P. Lyu, and L. Zhu, "Single- and dual-band high-order bandpass frequency selective surfaces based on aperture-coupled dual-mode patch resonators," *IEEE Trans. Antennas Prppag.*, Vol. 69, No. 4, 2130–2141, 2021.
15. Wang, D. S., P. Zhao, and C. H. Chan, "Design and analysis of a high-selectivity frequency-selective surface at 60 GHz," *IEEE Trans. Microw. Theory Techn.*, Vol. 64, No. 6, 1694–1703, 2016.
16. Ye, H., W. T. Dai, X. Chen, H. Zhang, S. W. Bie, and J. J. Jiang, "High-selectivity frequency-selective rasorber based on low-profile bandpass filter," *IEEE Antennas Wireless Propag. Lett.*, Vol. 20, No. 2, 150–154, 2021.